Geochimica et Cosmochimica Acta 336 (2022) 208–218

Contents lists available at ScienceDirect

Geochimica et Cosmochimica Acta

journal homepage: www.elsevier.com/locate/gca

Extreme lithium isotope fractionation in quartz from the Stewart pegmatite

Patrick R. Phelps *, Cin-Ty A. Lee

Dept. of Earth, Environmental and Planetary Sciences, Rice University, Houston, TX, USA

ARTICLE INFO

Article history:
Received 18 April 2022
Accepted 8 September 2022
Available online 15 September 2022
Associate editor: Fang Zhen Teng

Keywords:
Pegmatites
Lithium isotopes
Crystal growth

ABSTRACT

Pegmatites are magmatic bodies consisting of centimeter to meter sized crystals and can sometimes be a source for critical economic resources such as lithium (Li). Determining the chemistry and kinetics involved in pegmatite formation may be important for understanding the element enrichment process. Here, we analyzed the Li isotope compositions of quartz crystals from the Stewart pegmatite in southern California, USA. We find large Li isotopic fractionations: >40‰ between different crystals and >20‰ from core to rim in a single crystal. Two mechanisms for these extreme fractionations were considered: rapid crystal growth rate and Rayleigh fractionation. We find that although rapid crystal growth rate (1–10 m/day) can explain elemental variations, rapid growth alone is unable to explain the most extreme isotopic fractionations. Rayleigh fractionation can account for the largest isotopic fractionations if 96–99.9% of the Li is removed from the system through crystallization of lepidolite and spodumene, but alone cannot explain the observed elemental variability in the quartz. We thus suggest that both processes operated. Trace element enrichments may be more sensitive to growth rate while Li isotope ratios may be more sensitive to changes in the isotopic composition of the pegmatitic fluids during crystallization of the quartz.

1. Introduction

Within pegmatites are some of the largest crystals on earth, ranging from centimeters to a few meters in size. The pegmatite bodies, themselves, are typically found as dikes or lenses within plutonic bodies, and tend to be small (<1 m to ~100 m) compared to the km-scale sizes of plutons (London and Kontak, 2012). Often sourced from the plutons that surround them, pegmatites appear to be emplaced late, after much of the pluton has cooled and crystallized (Chadwick, 1958). Because of their late origins, pegmatites are typically highly enriched in incompatible components, such as water and many elements that are normally present in trace amounts in the host plutons (Chadwick, 1958; Jahns and Burnham, 1969). Their small sizes and their late origins indicate they cooled quickly compared to their host plutons (Chakoumakos and Lumpkin, 1990; Webber et al., 1999; Simmons and Webber, 2008). Small grain sizes are expected during rapid cooling (e.g., Cashman, 1993; Winkler, 1949), so the large crystal sizes in pegmatites seem paradoxical. Given the short lifespans of pegmatites, the large crystal sizes of pegmatite crystals require rapid growth (Simmons and Webber, 2008; Phelps et al., 2020). Exactly how fast and what mechanisms facilitate rapid crystal growth are of interest.

In a previous study, we documented rapid crystal growth in pegmatites through the presence of extreme trace element disequilibria in pegmatitic quartz crystals (Phelps et al., 2020). These quartz crystals are from miarolitic cavities in the Stewart pegmatite, a *gem*- and Li-bearing pegmatite in the Pala mining district in southern California, USA (Morton et al., 2018). The miarolitic cavities developed in chimney-like structures formed by hydrous fluids, which emanated from the core of the pegmatite and fractured upwards into the upper margin of the pegmatite. The fluids were water-rich and crystallized into an assemblage of muscovite, albite, lepidolite, tourmaline, and quartz.

Crystal growth is known to affect the concentrations of trace elements in a crystal (Tiller et al., 1953; Watson and Müller, 2009). At rapid growth rates compared to the rates of chemical diffusion in the host fluid, incompatible trace elements become enriched in the fluid boundary layer and the crystal inherits this enriched composition. Incompatible trace element concentrations in these quartz crystals were anomalously enriched, consistent with rapid crystal growth. We used the spatial distributions of trace elements (Al and Ge, specifically) within the quartz to

* Corresponding author.
E-mail address: prp2@rice.edu (P.R. Phelps).

https://doi.org/10.1016/j.gca.2022.09.014
0016-7037/

estimate crystal growth rates and showed that cm-scale quartz crystals may have grown within a few hours (Phelps et al., 2020).

One challenge of using trace element concentrations is separating kinetic effects from changes in the fluid composition itself, which may be externally driven by crystal fractionation or other processes. Here, we build on the previous study through an investigation of Li isotopes in quartz. Isotope fractionation can arise from both equilibrium and kinetic effects. At equilibrium, isotopic mass differences lead to energetic differences in how the isotopes are partitioned into a crystal, resulting in a small isotopic fractionation during crystallization. After extensive crystallization, the integrated effects can lead to extremely fractionated residual fluids if previously crystallized products are unable to re-equilibrate with the fluid as is often the case due to slow solid-state diffusion (e.g., Rayleigh fractionation). Late-forming crystals inherit this fractionated signature from the fluid. Kinetic fractionation, on the other hand, is caused by isotopic differences in diffusivity within the fluid. Such differences drive isotopic fractionation through differences in the diffusive transport of each isotope. The effect is most pronounced when crystal growth rate exceeds the rate of diffusive transport of a given trace element in the fluid (Tiller et al., 1953; Smith et al., 1955; Watson and Müller, 2009; Watkins et al., 2017). Our work focuses on Li systematics because Li is abundant in the pegmatitic fluids of interest and is one of the few incompatible elements that are enriched to measurable quantities in quartz. Its two isotopes, ^{7}Li and ^{6}Li, also have one of the largest relative mass differences for a single element, maximizing the possibility of measurable kinetic isotope effects (Kunze and Fuoss, 1962; Richter et al., 2006). Because ^{6}Li diffuses faster, rapid crystal growth leads to enrichment in ^{7}Li within the fluid boundary layer, resulting in the crystal also becoming heavier with progressive growth.

Here, we report pegmatitic quartz with extremely large inter- and intra-crystalline Li isotope variation. We show that both Rayleigh fractionation and kinetic effects are needed to explain the heavy isotopic ratios. These extreme fractionations highlight the fact that care must be taken in interpreting stable isotope fractionations at the micron scale, where these fractionation processes are magnified.

2. Geological background

The Stewart pegmatite is a subhorizontal Li-bearing dike emplaced within an olivine-hornblende gabbro associated with the Cretaceous northern Peninsular Ranges Batholith. The dike was dated to be the same age as the host gabbro and is thus interpreted to have derived as late-stage residual fluids associated with crystallization of the host gabbro (Morton et al., 2018). The dike exposure is ~1.1 km long with a maximum thickness of 56 m. According to Morton et al. (2018) and Jahns and Wright (1951), the pegmatite consists of six distinct layers. These are in ascending order: (1) an aplitic footwall zone consisting of K-feldspar, albite, and quartz; (2) a lower intermediate zone of pegmatitic texture consisting of schorl, muscovite, perthite, and albite; (3) a core zone, which houses many of the lithium-bearing phases, such as spodumene, lepidolite, amblygonite, lithiophilite, petalite, and heulandite, as well as quartz, albite, muscovite, K-feldspar, and elbaite lenses; (4) a perthite zone, which houses vertical chimney structures containing *gem*-bearing (elbaite and kunzite) miarolitic cavities; (5) an upper intermediate zone consisting of graphic granite (intergrown quartz and K-feldspar), schorl, perthite, and muscovite; and (6) a hanging wall zone, consisting of platy muscovite with intergrown small elbaite, graphic granite, and schorl.

The quartz from this study comes from the miarolitic cavities in the chimneys that were emplaced into the perthite zone (zone 4). All quartz studied here are from the same cavity. The chimneys are believed to have formed after the perthite zone had mostly crystallized and while the central core zone of the pegmatite body was still crystallizing (Morton et al., 2018). Fluid exsolution and pressurization sourced from the core zone hydraulically fractured the perthite zone, leading to the chimneys and the fluids from which the quartz in this study (and other gems) grew (Phelps et al., 2020).

3. Methods

Quartz crystals D, F, and G from the Stewart pegmatite were cut, mounted in epoxy, and polished before being imaged at Rice University using cold cathodoluminescence (CL). CL uses electrons to excite defects in a crystal, which then luminesce with visible light at the site of the defects (e.g., Götze et al., 2005). A 12 kV accelerating voltage was used with a vacuum current of 0.4–0.5 mA and a camera exposure of 4 s. One was analyzed in a previous study (crystal F; Phelps et al., 2020) with the same analytical conditions. CL images of the quartz crystals are shown in Fig. 1.

These crystals were then analyzed at the California Institute of Technology using secondary ion mass spectrometry (SIMS) with a Cameca IMS 7f-GEO. In separate analyses, we measured δ^{7}Li values as well as concentrations of Li, Al, and Ge. For isotopic analyses, a spot size of ~30 μm was adopted. For low concentration portions of the crystals, we used a 10 nA beam current, and 1.5–3 nA for higher concentration regimes. Approximate concentrations were known from previous work, which helped guide isotopic measurements (Phelps et al., 2020). The dwell times were 3 s for ^{6}Li and 1 s for ^{7}Li with 20–80 cycles per analysis. The mass resolving power was ~1000 to resolve ^{7}Li from ^{6}LiH. Throughout, we used an accelerating voltage of 8.5 kV.

For concentration analyses, we rastered an area of 15 μm before taking a 10 μm spot measurement. A 10 nA beam current was used for all analyses. A dwell time of 1 s was used for Li, Si, and Al and 4 s for Ge. Each point had 15 cycles. For isotopic analyses, standards GSD-1G and GSE-1G (Jochum et al., 2005) were measured before and after each analytical run to obtain instrumental mass fractionation factors. These fractionation factors were applied to the quartz samples. However, we note that the standards and the quartz samples have different matrices, and without an independent quartz standard, we did not apply a matrix correction. We have gone ahead to report our values with respect to the LSVEC standard, but we note that our analyses may be systematically biased. Relative differences between and within quartz samples, however, are robust. At the points where dedicated isotopic ratios were measured, Li concentrations were estimated by plotting the ratio of ^{7}Li and ^{6}Li signal intensities normalized to beam current against known concentrations of the isotopic standards (see Fig. S1). For dedicated concentration determination, we monitored ^{74}Ge, ^{7}Li, ^{27}Al, and ^{28}Si (internal standard) and used NIST-610 and NIST-612 glasses as external standards (Pearce et al., 1997).

To determine the deadtime correction, we analyzed two standards with the same δ^{7}Li values but different Li concentrations at the same beam current. Deadtime—the amount of time after a detector counts an ion before it can count another—was adjusted until the δ^{7}Li values were the same. Using GSE-1G and GSD-1G, which have a δ^{7}Li ~31‰ and a factor of 10 difference in Li concentration, and a 1 nA beam current, we found a deadtime correction of 38 ns. We then measured a spot on each standard at 10 nA and reproduced the correct isotopic value within 1‰.

4. Results

4.1. Cathodoluminescence

The quartz crystals from the Stewart pegmatite have been shown to have three distinct CL color zones: a white core zone sur-

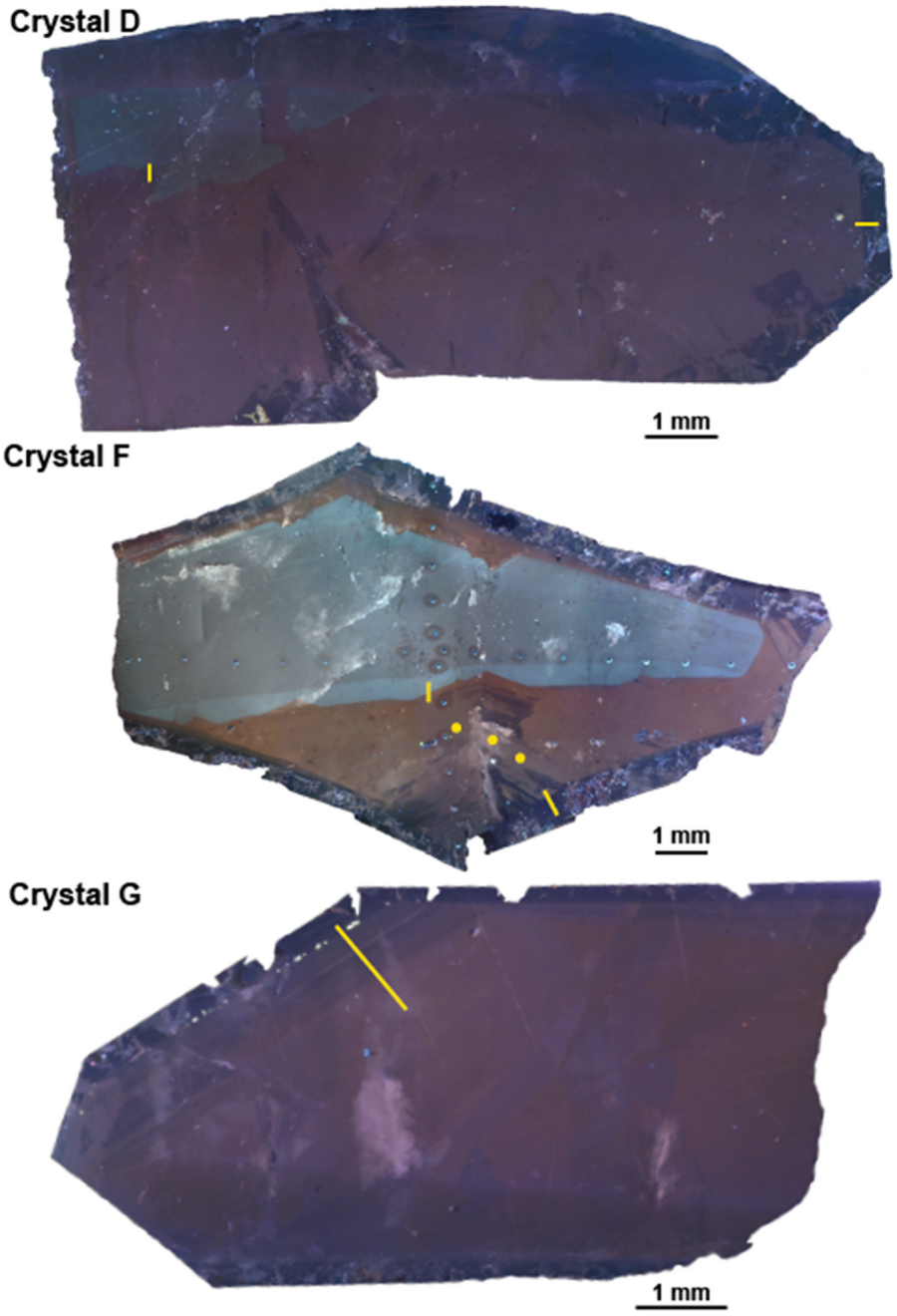

Fig. 1. Cathodoluminescence images of quartz crystals. Three quartz crystals from the Stewart pegmatite imaged using cold cathodoluminescence (CL). Crystal D has three CL color zones: a white core area, an orange intermediate zone, and a purple rim. Yellow lines indicate areas where SIMS analyses were done in all crystals. Crystal F also shows the three color zones. Crystal G only exhibits two CL color zones: an orange zone surrounded by a purple core. (For interpretation of the references to color in this figure legend, the reader is referred to the web version of this article.)

rounded by an orange zone and a purple rim (Phelps et al., 2020). Crystal D shows the same color patterns, while G only luminesces purple and orange zones (see Fig. 1). In D and G, the CL colors are of lower intensity than in F. While we were not able to measure the emission spectra of the quartz, some possible controls on color are as follows. As explained in Götze et al. (2001), orange CL in quartz is often caused by non-bridging oxygen hole centers. Violet is caused by AlO_4/M^+ centers where M^+ is often Li^+, H^+, or another 1 + cation. Therefore, the purple color may be the result of an overlap of these two defects. The white color may also be a mixture of defects.

4.2. Lithium isotopes and concentrations

In each crystal, we characterized the Li isotopic ratios within the different CL color zones and across the zone transitions. As seen in Fig. 2, each crystal has a >20‰ increase from core to rim with D varying from 12 to 34‰, F increasing from 11‰ to 37‰, and G increasing from 31‰ to 55‰. The core values of D and F are similar to those found in bulk rock pegmatites and granites, while the rim values and all zones in G are significantly higher, matched only by materials formed during weathering and sedimentary processes. As noted in the Methods section, our use of basaltic glasses as

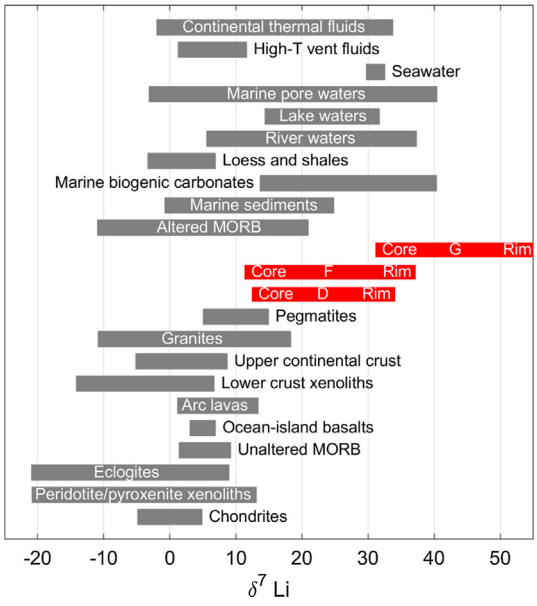

Fig. 2. Li isotope ratio comparisons. The Li isotope ratios from three quartzes from the Stewart pegmatite are compared to Li isotope compositions of other types of materials. Values from this study may be some of the highest Li isotope ratios measured (Tang et al., 2007; and references therein; Altered MORB: Tomascak et al., 2016; Eclogite: Marschall et al., 2007). We note the absolute Li isotopic composition may be different than what is reported due to standards mismatch; although, we are confident in the relative inter- and intra-crystalline differences. See text for details.

external isotopic standards may introduce a systematic bias in the absolute isotopic composition of the quartzes due to matrix effects. We note that matrix effects (non-crystalline vs crystalline) between quartz and quartz glass have been shown to be minimal for oxygen isotopes (Eiler et al., 1997). Whether this also holds for Li isotopes is unclear as compositional differences are known to cause instrumental Li isotopic fractionations (e.g., Bell et al., 2009; Hoover et al., 2021). For all subsequent discussions, we report the absolute Li isotopic compositions (normalized to LSVEC), but the reader is cautioned that there may be a systematic bias in the absolute values that we have not accounted for. A dedicated study with Li isotope quartz standards would need to be conducted to assess the extent of systematic bias in Li isotope values for quartz. However, the *relative* differences in isotopic ratios between and within the quartz samples are robust. Concentrations are also robust as matrix effects for concentrations are small.

The detailed structure of isotope transects are also of interest. In Fig. 3, isotopic ratios and corresponding concentrations are plotted versus distance in each crystal. A key observation is that there is no obvious correlation between δ^7Li and Li concentration for crystals D and F. Across the orange to purple CL transition in D, Li concentration rises abruptly from <20 to >70 ppm and then continues to rise to 115 ppm through the purple zone. In contrast, δ^7Li decreases slightly (from 32‰ to 29‰) across this transition. Similar systematics are seen across the white to orange transition in D: concentration increases abruptly across the transition from a few ppm to >10 ppm, but δ^7Li remains relatively constant from 25‰ to 30‰ except for a localized dip to 11‰ near the transition. Similar systematics are also seen in crystal F, although the isotopic composition is more variable. Li concentration increases from <10 to ~25 ppm across the white to orange transition and increases again (from ~50 to ~200 ppm) across the orange to purple transition. δ^7Li in F varies between 15 and 29‰ in the white zone, then decreases to ~12‰ in the orange zone. This is followed by an outward increase to ~20‰ in the middle of the orange zone and up to ~30‰ at the edge of the orange zone before finally increasing to ~35‰ within the outer purple zone. Unlike the decoupled element-isotope systematics in crystal D and F, concentration and isotopic ratios in G appear to correlate as both increase from core to rim. Despite this coupled behavior within the crystal, G overall has the heaviest δ^7Li (30–55‰) and lowest Li concentrations (4–8 ppm) of the three crystals. Li concentrations in crystal F broadly follow the same color patterns in other quartz grains (white <10 ppm, orange ~40 ppm, and purple ~200 ppm) in a previous study (Phelps et al., 2020).

Concentration and isotopic compositions are plotted against each other in Fig. 4 to further elucidate any relationships between Li and δ^7Li. We plot each crystal with a unique symbol and use colors to reflect corresponding CL color zone (white, orange, and purple zones denoted by gray, orange, and purple, respectively). Three groupings are evident. Group 1 manifests as a steeply sloped trend in δ^7Li versus Li space with a large range in δ^7Li (11–55‰) over a small range in concentration (1–10 ppm). This group includes all three crystals and all color zones but is primarily defined by data from crystal G and the core zones of D and F. Group 2 manifests as a much shallower trend with a small change in δ^7Li (25–35‰) over a large change in Li concentration (18–210 ppm). Interestingly, Group 2 primarily includes the purple and orange zones from crystals D and F. Group 3 is represented by a small cluster of data from crystal F centered around δ^7Li of 15‰ and Li of ~25 ppm.

In our previous work, we showed that Li and Al correlate strongly in quartz due to a coupled substitution for Si (Phelps et al., 2020). We thus investigated the relationship between Li and Al at a few points within each crystal. In Fig. 5, we plot atomic Li/Al ratio against Li concentration in ppm by weight. The atomic % is relative to the whole quartz (i.e., *mol* Li/(*mol* SiO_2 + *mol* Li) × 100). In all cases, we note that at low Li concentrations, Li/Al positively correlates with Li concentration albeit with different slopes (see Supplementary Fig. S2). We note that in both crystals D and F, Li/Al saturates at ~0.6 atomic Li/Al. Crystal G does not appear to reach saturation, but Li/Al and Li concentrations are an order of magnitude lower than for D and F.

5. Discussion

5.1. Comparison to Li isotopic compositions of terrestrial materials

In Fig. 2, the individual crystal values are compared against δ^7Li of different geological materials compiled from the literature. Our compilation builds on that from Tang et al., (2007; and references therein) and includes: igneous rocks ranging from primitive (ultramafic and mafic) to highly evolved compositions (granites) and materials from low temperature systems, such as weathered rocks, soils, sediments, and different types of meteoric waters. The heaviest isotopic compositions in the quartz exceed the highest reported values for any igneous rocks, assuming our values are not systematically biased by >40‰ due to compositional and/or matrix effects as discussed above. The lighter end of the pegmatite quartz overlaps with the heaviest values reported so far for igneous rocks, consisting mostly of granitic endmembers. Overall, the heavy δ^7Li of the pegmatite quartzes are more similar to those from low temperature aqueous fluids, sediments, or weathering products, but the heaviest values observed here are still higher than these low temperature materials.

In detail, we note that the cores of quartz crystals D and F are heavier than the mean of pegmatites (~10‰) compiled from the literature (Fig. 2). Assuming equilibrium and an equilibrium fractionation factor between quartz and aqueous fluid of α = 1.010 (Lynton et al., 2005), the cores of crystals D and F (white zones in Fig. 3) would have been in equilibrium with a fluid of a δ^7Li

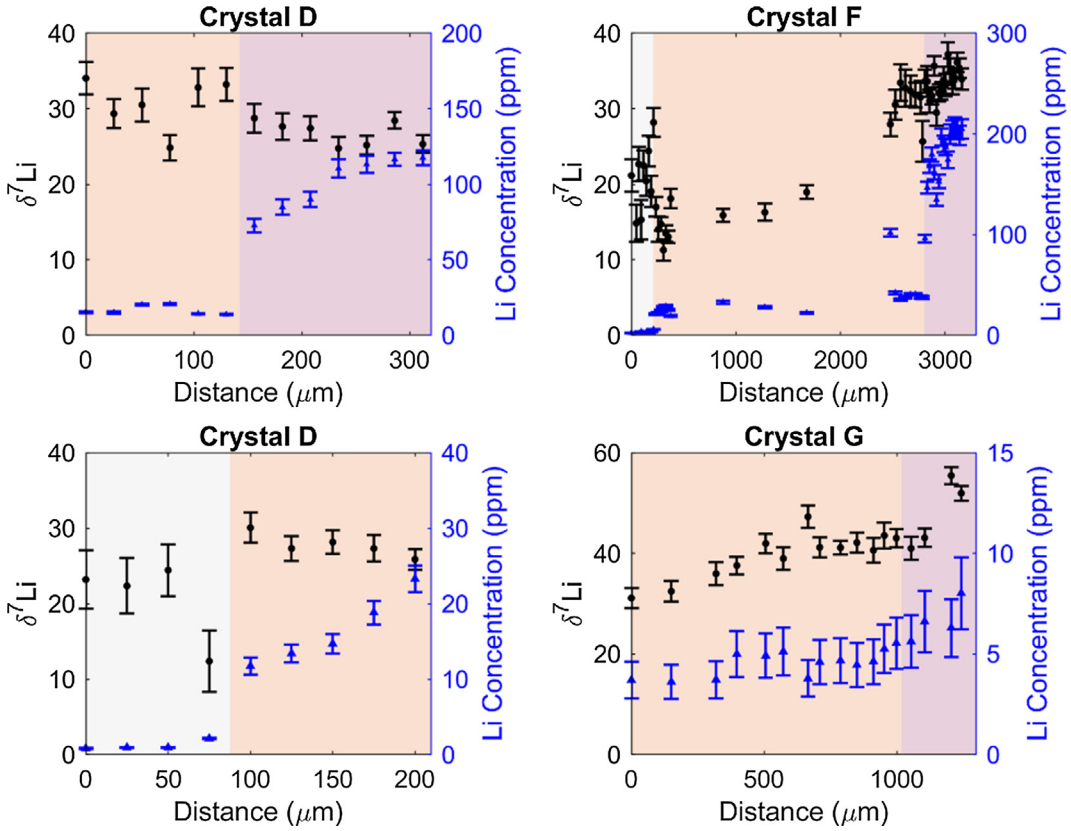

Fig. 3. Li isotope ratios and Li concentrations vs distance. Li isotope ratios (black circles) as well as Li concentrations (blue triangles) are plotted against distance inside each crystal (rim to right). Background colors in each plot correspond with CL color zones as shown in Fig. 1. Letters at top of each panel corresponds to the name of the crystal. Please see Fig. 6 for a larger version of crystal F. Error bars for isotopic ratios are 2 times the standard error of the mean. Error bars for the concentrations are $2 \times \sqrt{\sigma_{slope}{}^2 + \sigma_{counts}{}^2}$, where σ_{slope} is the standard error of the conversion factor from the number of counts/current to concentration (i.e., the standard error of the slope), and σ_{counts} is the standard error of the number of counts/current. (For interpretation of the references to color in this figure legend, the reader is referred to the web version of this article.)

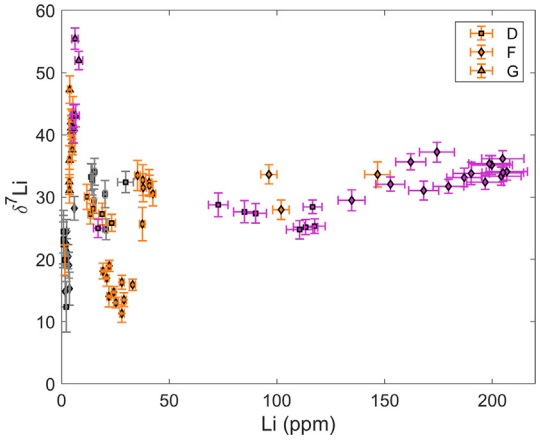

Fig. 4. Li isotope ratio vs Li concentration. Li isotope versus Li concentration from Fig. 3 for all crystals. Black squares correspond to crystal D, circles are for crystal F, and triangles are for crystal G. The colors correspond with CL color zones (gray is the white core, orange is the orange zone, and purple is the purple zone). Error bars are the same as those in Fig. 3. (For interpretation of the references to color in this figure legend, the reader is referred to the web version of this article.)

10–11‰—similar to average pegmatites. Assuming the quartz are always in equilibrium with their growth fluid, the higher rim compositions indicate the fluid composition was higher than average pegmatites. Determining the origin of the high isotopic ratios will be discussed further.

Since pegmatites represent the last and most fluid-rich portion of a magmatic system to crystallize, we expect them to be the most isotopically fractionated products formed during magmatic differentiation. Because the lighter isotope preferentially occupies higher coordination sites, differences in the coordination number of silicate minerals, fluids, and silicate melt can lead to isotopic fractionation of the melt/fluid (Wunder et al., 2006). For example, Li is 4-fold coordinated in aqueous fluids and silicate melts (Lyubartsev et al., 2001), but in 5- and 8-fold coordination for most silicate minerals (e.g., Deubener, Sternitzke, & Mueller, 1991; Penniston-Dorland, Liu, & Rudnick, 2017). Thus, fractionation of spodumene and alkali feldspar, which are isotopically light, leaves behind heavy Li in the residual melt/fluid. However, Li in quartz, which is otherwise extremely depleted in Li, occupies either 2- or 4-fold coordination sites (Sartbaeva et al., 2004; Maloney et al., 2008), so quartz Li isotopic compositions are likely similar to or only slightly higher than the melt/fluid itself (Teng et al., 2006), which is in line with an equilibrium fractionation factor of 1.01.

5.2. Evidence for Al limiting Li incorporation

Our previous work on these quartz crystals tied the concentrations of certain trace elements, such as Al and Ge, to crystal growth rate (Phelps et al., 2020). However, for Li, Fig. 3 shows Li isotopes and concentration are not strongly correlated. Crystal G shows some correlation, but a rise in isotopic ratio does not occur near a CL boundary, where there is a change in concentration of Li

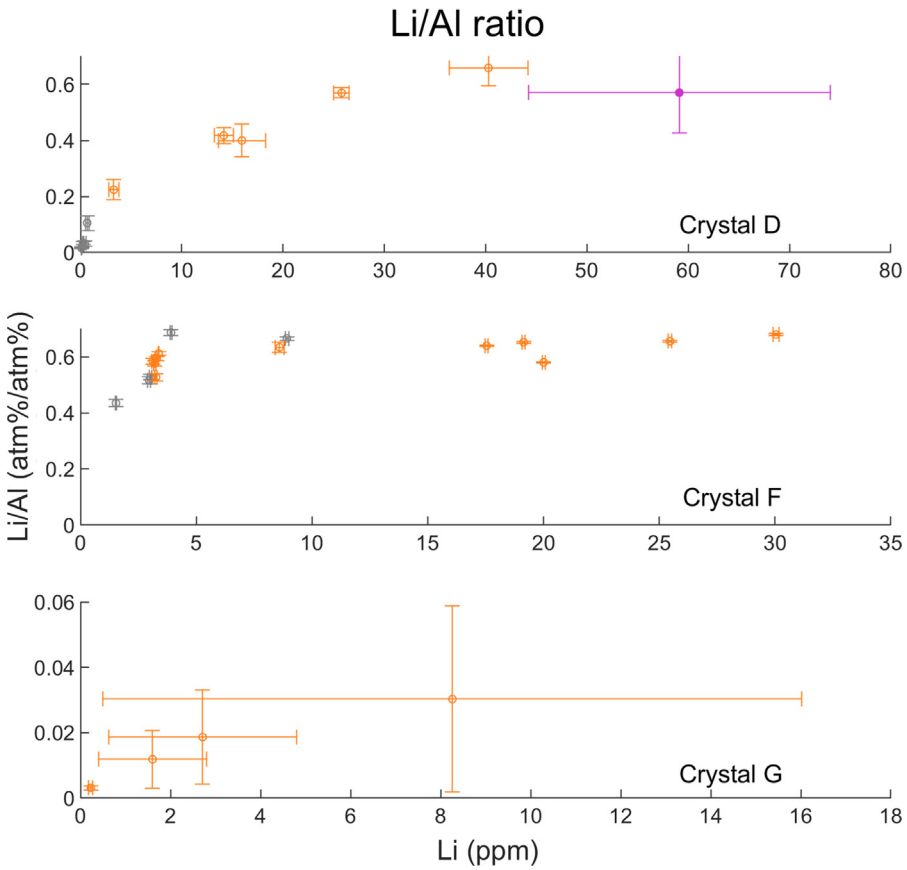

Fig. 5. Ratio of Li to Al vs Li. The atomic ratio of Li to Al is plotted against Li in ppm by weight for each crystal. As in Fig. 4, the colors of the data points correspond to the CL color zones. Letters on lower right corner of each panel correspond to name of crystal. Error bars are 2 times the standard error of the mean.

and other incompatible elements like Al. This lack of correlation suggests that the Li isotopic ratios and Li may not be governed by the same processes that control the concentrations of Ge and Al or may be governed by multiple processes.

To gain more insight into the underlying process affecting Li concentration, we examine Li/Al ratios (Fig. 5). Li/Al ratios initially increase with increasing Li concentration but then plateau at a constant Li/Al ratio. This plateauing of Li/Al ratio at high Li concentrations suggests that Al incorporation is not limited by Li, but Li is instead limited by the amount of Al present. That is, Li cannot exceed the number of compensating charge sites offered by Al. At low concentrations of Li, Al is in such excess that Li concentration increases without Al-limitation, but at high concentrations, available sites associated with Al are filled. Al may be necessary for Li to be incorporated into the quartz. We conclude that Li concentration profiles may not be directly controlled by crystal growth rate. Instead, Li concentration in the quartz may be controlled by a combination of Li concentration in the fluid and the incorporation of Al into the crystal, which itself is controlled by growth rate owing to the slow diffusivities of Al (Phelps et al., 2020).

Further evidence exists of Li and Al being coupled within the quartz. The solid state Li diffusivity in quartz may be as high as 1.1×10^{-12} m^2 s^{-1} at 500 °C (Verhoogen, 1952), yet Al diffusivity in quartz is 9×10^{-25} m^2 s^{-1} (Tailby et al., 2018). Li concentration gradients would relax completely in the quartz crystal at 500 °C in less than a year (5 mm diffusion distance). However, Al would take over 100 million years at this temperature to relax over a 100 μm distance. Since Li gradients still exist within the crystal and because they closely resemble Al concentration profiles (Phelps et al., 2020), Li is likely coupled with Al in the quartz. This does not necessarily mean Li isotope incorporation is controlled by Al.

5.3. Exploring a kinetic origin for heavy δ^7Li

One possible cause of high Li isotope fractionations is rapid crystal growth (Jambon, 1980; Maloney et al., 2008; Watson and Müller, 2009; Watkins et al., 2017). During growth, the quartz will tend to reject Li (Neukampf et al., 2019), causing it to build up directly in front of the growing crystal surface. If growth is slow relative to diffusion of Li in the melt, the increase in Li will relax to the far field concentration through diffusion. Conversely, if growth is sufficiently fast, the Li concentration will increase in the boundary layer surrounding the crystal. Assuming local equilibrium holds at the immediate contact between melt and crystal surface, then the crystal will inherit the high Li concentration of the boundary layer, eventually becoming enriched itself.

To model this in our quartz, we analyze how a step change in growth rate at the white to orange transition in the crystal influences the isotopic ratio, following the framework set up in Phelps et al. (2020), which follows from Smith et al. (1955). We assume that crystal growth prior to the transition is at steady state, meaning that the crystal growth rate and the nature of the boundary layer are initially constant with time. At the CL color transition, we consider a step change in crystal growth rate, from one constant rate to a higher constant rate. This general model setup is solved analytically by Smith et al. (1955). By treating each isotope independently with different diffusivities but having the same partition coefficient (i.e., no equilibrium fractionation between the boundary layer and quartz, only diffusive fractionation), we model how the concentrations of each isotope changes, depending on the magnitude of the increase in crystal growth rate.

We compare the measured isotopic ratios of crystal F to the modeled isotopic ratios based on crystal growth rate fractionation

in Fig. 6. Key to the modeling are the initial and final growth rates (before and after the step change in growth rate), the partition coefficient of Li into quartz (k), and the diffusivities of the isotopes. This model assumes a sudden increase in growth rate occurs at the white to orange transition from 10^{-7} to 10^{-5} m s^{-1} (Phelps et al., 2020). We plot two sets of model outputs for two different values of k because the exact Li partition coefficient k into quartz is unknown for our system. We use 0.3 and 0.02 for k as those are the values for Li (Neukampf et al., 2019) and Al (Nash and Crecraft, 1985) in rhyolitic systems, respectively. If Li is not strongly coupled to Al in the melt, then we expect it to behave closer to this higher partition coefficient. However, if there is a strong coupling, then Al may govern how easily Li partitions into quartz. We expect the true partition coefficient to lie somewhere in between. To determine ^{6}Li diffusivity, we relate it to the ratio of isotope masses through the following equation (Jambon, 1980; Bearman and Jolly, 1981):

$$\frac{D^{Li^6}}{D^{Li^7}} = \left(\frac{m^{Li^7}}{m^{Li^6}}\right)^{\beta}. \quad (1)$$

The power β defines the difference in diffusivity. An ideal gas follows Graham's law, i.e., $\beta = 0.5$ (e.g., Richter et al., 2006), which can be derived from kinetic gas theory and is the theoretical upper limit. We assume the diffusivity of ^{7}Li in the fluid is that for bulk Li of 1.87×10^{-8} m^2 s^{-1} at 500 °C (Nigrini, 1970) and calculate the diffusivity for ^{6}Li based on β and this value.

For a given k and a change in growth rate from 10^{-7} to 10^{-5} m s^{-1} we have plotted diffusion-driven fractionation curves for different values of β. The lowest possible values of β are 0.01475 (Richter et al., 2006) and 0.072 (Fritz, 1992) for Li diffusion in aqueous solutions. For an intermediate value, we use 0.215, which was reported for a silicate liquid (Richter et al., 2003). We note that the compositions of fluids in these experiments differ from natural pegmatitic fluids, so there is considerable uncertainty in applying them to our study. In any case, if the quartzes crystallized from a water-rich fluid/melt that exsolved from a silica-rich magma, the appropriate β to use in our diffusion-driven fractionation models probably lies between that of a pure aqueous fluid and a silicate melt (~0.02–0.2). However, to reproduce the highest δ^7Li observed in the quartzes by differences in ^{6}Li and ^{7}Li diffusivities in the fluid, β values closer to a silicic magma (e.g., ~0.2) or higher (e.g., ~0.4) as well as partition coefficients closer to Al (e.g., ~0.02) than that of Li are required. While the high rim δ^7Li can be modeled using a high β, the lower δ^7Li values within the middle of the orange zone are then over-estimated. Instead, the low δ^7Li of the orange zones are predicted with the low β more relevant for aqueous systems.

Isotopic changes in the orange zone could conceivably be related to an increase in crystal growth rate. The extreme fractionations seen in the outer parts of the crystals, however, cannot be explained by the same increase in growth rate used to explain the orange zones. One possibility to explain the more extreme fractionations is to allow for an acceleration of growth rate (rather than a change to a constant growth rate), but such a model would be too unconstrained, leading us not to pursue it here. Another possibility, which we explore next, is changes in the bulk fluid composition during quartz crystallization.

5.4. Exploring Rayleigh fractionation for the origin for heavy δ^7Li

In this section, we consider the effects of a fluid composition on the Li isotopic composition of the quartz. We assume local equilibrium, wherein the quartz equilibrates with the growth medium, a hydrous fluid or a silicate melt. We begin by focusing on Li isotope versus Li concentration systematics in quartz shown in Fig. 4, wherein different arrays are seen for the different quartz zones (a steep slope for crystal G and shallow slopes for D and F). This

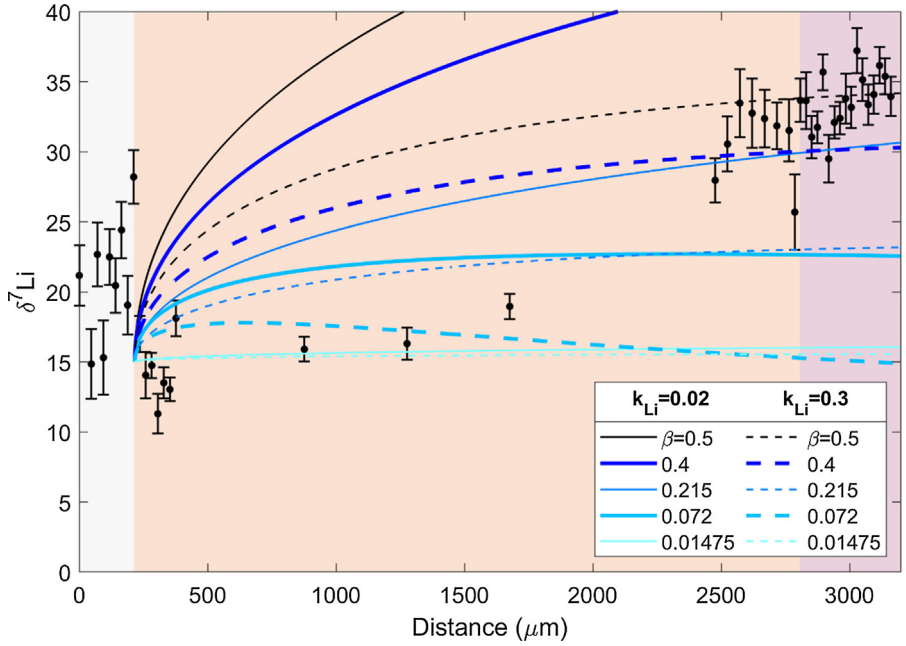

Fig. 6. Kinetic crystal growth model. Li isotope ratios are predicted using a kinetic fractionation model based on crystal growth physics for crystal F. All model lines are dependent on the partitioning of Li into quartz, the difference in diffusivity between ^{6}Li and ^{7}Li in the growth fluid (^{6}Li diffuses faster), and crystal growth rate. Solid lines correspond to a partition coefficient (k) for Li in quartz of 0.02, which is the value for Al in quartz. Dashed lines are for k = 0.3 from Neukampf et al. (2019). Calculations are done for different β values in Eq. (1) used to estimate differences in diffusivities. β values closer to 0 indicate less disparity in diffusion speeds. β = 0.5 is the theoretical upper limit of an ideal gas, β = 0.4 is shown for reference, β = 0.215 is the value for rhyolitic melt (Richter et al., 2003), β = 0.072 is one measurement within an aqueous fluid (Fritz, 1992), and β = 0.01475 is another measurement within an aqueous fluid (Richter et al., 2006). Each model assumes an instantaneous change in growth rate from 10^{-7} to 10^{-5} m s^{-1} after crossing the white to orange CL transition. Error bars are 2 times the standard error of the mean. (For interpretation of the references to color in this figure legend, the reader is referred to the web version of this article.)

may suggest the growth environment was changing as the crystals were growing with the different slopes meaning the crystals were growing at different times. Maloney et al. (2008) conducted a study of Li isotopes in tourmaline in pegmatites and concluded the changes in slope seen in δ^7Li vs Li space are caused by changes in the composition of the growth medium. Here, we explore whether Rayleigh fractionation could cause the variations in isotopic composition.

Crystallization can cause large isotopic fractionations, particularly after large extents of crystallization. We model this process by Rayleigh distillation, which assumes fractional crystallization, wherein crystallized products physically segregate out of the system or, because of the slow rates of solid-state diffusion, crystals are unable to re-equilibrate with the fluid. The Rayleigh distillation equation describes isotope fractionation as

$$\frac{R}{R_0} = f^{\alpha-1}, \tag{2}$$

where f is the fraction of Li remaining, $R = C_7/C_6$ with R_0 being the initial ratio (f = 1), and α is the isotopic fractionation factor. The fractionation factor reflects subtle differences in the equilibrium partition coefficient between the two isotopes. Eq. (2) can be re-expressed in terms of delta notation:

$$\frac{\delta^7Li + 1000}{\delta^7Li_0 + 1000} = f^{\alpha-1}. \tag{3}$$

When isotope ratios are plotted versus the logarithm of f, Rayleigh distillation is expressed as a straight line with a slope of $\alpha - 1$ (see Fig. 7). By normalizing to a local initial isotopic composition, any fractionation sequence can be compared on the same plot. For each crystal, we take the core composition to represent the initial and the rim to represent the last stage of crystallization. The difference in isotopic composition between rim and core (left hand side of Eqs. (2) and (3)) can then be used to estimate the fraction of Li remaining in the fluid f.

We have taken Eq. (3) and plotted Rayleigh distillation curves in Fig. 7 for α = 0.996 (Wunder et al., 2006) and α = 0.994 (Wunder et al., 2007), which correspond to mineral-melt fractionation factors for spodumene and lepidolite, two Li-bearing silicate minerals that crystallized before and during the crystallization of the quartz in the miarolitic cavities. These two minerals are the largest Li sinks in our system and should be the most significant moderators of the Li isotopic ratios. Assuming the Li in the quartz came from fluids that were growing spodumene and/or lepidolite, we can

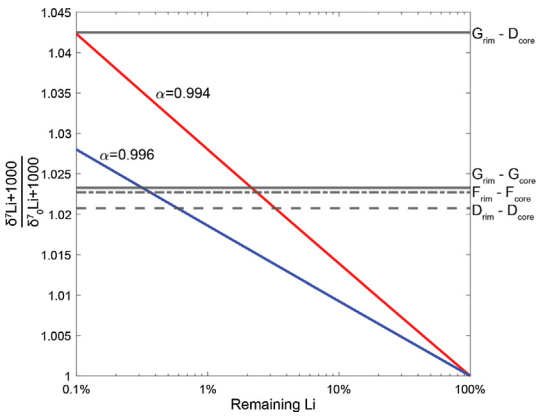

Fig. 7. Rayleigh fractionation model. Model outputs of Li isotope ratio versus fraction of remaining Li for different equilibrium isotope fractionation factors α (red and blue lines). Horizontal lines show the difference between rim and core isotopic compositions for crystals D, F, and G. (For interpretation of the references to color in this figure legend, the reader is referred to the web version of this article.)

determine how much Li must be removed from the system to produce the fractionations observed in the quartz rims. For crystals D and F, we assume the growth fluid was initially in equilibrium with the quartz cores. Their isotopically heavy rim values would indicate that between 96% and 98% of Li was removed if lepidolite was the Li sink and 99–99.7% if spodumene was the sink. If we assume the fluid from which crystal G grew also was initially in equilibrium with its core, then it crystallized over a similar interval. If, however, its fluid was initially in equilibrium with a composition similar to D's core, then 99.9% removal of Li is required to produce its rim values. Based on the δ^7Li versus concentration plots in Fig. 4 and the foregoing discussions, crystal G may well have been initially growing from a fluid of similar concentration and isotopic ratio as D and F. If so, crystal G's higher core measurements indicate it may have started growing after the fluid had fractionated significantly. This is also in line with the steeper slope observed in δ^7Li vs Li space.

5.5. Other possible origins for heavy δ^7Li

While we can explain the large isotopic excursions using growth rate modeling and Rayleigh distillation, other possible explanations exist, including outcrop scale diffusion of Li, heterogeneity within the chimneys, and further fluid influx events. We first consider outcrop scale diffusion (Teng et al., 2006a, 2006b). Morton et al. (2018) analyzed whole rock pegmatite samples along a 45 cm section across a chimney within the perthite zone. They found Li concentrations to be locally enriched on the margins of the chimney (where quartz, muscovite, and K-feldspar are concentrated). If a significant amount of outcrop scale diffusion had occurred during or after growth of the miarolitic quartz, we might expect to see more diffuse lithium profiles.

We also consider heterogeneity within the chimneys. Bulk rock Li concentrations indeed vary across a given chimney (Morton et al., 2018), so it is possible that quartz crystals could have come from different sectors within a given chimney. Such heterogeneity could explain the differences between the isotopic and elemental compositions of our different quartz grains. For example, a crystal grown in the center of the cavity might incorporate lower concentrations of Li and high δ^7Li (e.g., crystal G), while those crystallized on the margins of the cavity might be richer in Li and isotopically lighter (e.g., D and F). These different growth zones may also be evident in the δ^7Li vs Li groups, with different areas of the chimney producing different slopes or clusters in δ^7Li-Li space.

Finally, there is also the possibility of multiple influx events into the chimneys as a cause of the heavy δ^7Li. Evidence of multiple generations of quartz growth exist (Morton et al., 2018). What caused these nucleation and growth events is unknown, but further opening events of the same chimney could cause pressure fluctuations leading to new quartz growth. This process complements our proposed Rayleigh fractionation explanation, as the new fluids would be further fractionated from the core zone where spodumene and lepidolite are dominantly growing. This also could help explain the discontinuous nature of some of the Li isotopic profiles.

5.6. Origin of small-scale isotopic excursions by post-crystallization solid state diffusion

Superimposed on the broader isotopic variations across the quartz crystals are much smaller lengthscale isotope excursions that occur at the 50 μm-scale across a CL color transition, such as across the white to orange CL color transition in D and across the orange to purple transition in F. These isotopic excursions are manifested as dips on the lower Li concentration side of the transition. These small lengthscale excursions are superimposed on

the broader isotopic changes that occur across the crystal itself and cannot easily be explained by the above modeled changes in crystal growth rate or fluid composition.

We explore here the possibility that post-crystallization solid state diffusion of Li isotopes may have played a role. The faster diffusivity of ^{6}Li relative to ^{7}Li causes decoupling of the isotopes. While both diffuse down a concentration gradient, ^{6}Li diffuses faster into the low Li concentration zone. This decoupling results in an initial decrease in ^{7}Li/^{6}Li in the immediate vicinity of the concentration gradient, itself established during crystal growth. With time, of course, the isotopic excursion migrates further away from the initial concentration gradient and becomes more muted as the diffusion fronts of the two isotopes migrate.

We can quantify the above concept using a 1D diffusion model in the form of a diffusion couple, where we assume a step change in concentration but a constant initial isotopic ratio across this step. We use the analytical solution for an infinite half-space (Jaeger and Carslaw, 1959; Zhang, 2008):

$$C_{6,7} = \frac{C_L + C_R}{2} + \frac{C_R - C_L}{2} erf\left(\frac{x}{2\sqrt{Dt}}\right), \quad (4)$$

where $C_{6,7}$ is the concentration of ^{6}Li or ^{7}Li, $C_{L,R}$ corresponds with the initial concentration on the left and right sides of the step, D is the solid-state diffusivity of ^{6}Li or ^{7}Li, x is distance from the interface, and t is time. For our model results shown in Fig. 8, we used a step change in concentration from 1 to 15 ppm with a constant initial isotopic ratio of 27‰ to match the values from crystal D. Eq. (4) is then used for each isotope with their respective diffusivities from Eq. (1) to calculate the concentrations of each isotope through time and space. These concentrations are then converted back to the isotopic ratio through

$$\delta^{7}Li = \left(\frac{C_7/C_6}{12.1729} - 1\right) \times 1000, \quad (5)$$

with 12.1729 being the LSVEC standard ratio (Qi et al., 1997). The isotopic ratio can then be calculated versus distance at any time if Li isotope diffusivities are known.

Li diffusion in naturally occurring quartz is not well constrained. The study by Verhoogen (1952) analyzes how quickly Li can diffuse into quartz from a high Li source but does not analyze how Li already present in quartz diffuses. While this provides an upper bound on the diffusivity (1.1×10^{-12} m^2 s^{-1} at 500 °C, a temperature chosen to reflect the conditions of the pegmatite's genesis and based on Ti in quartz thermometry (Wark and Watson, 2006; Phelps et al., 2020)), it does not account for any coupling or competition of Li diffusion with other ions. Based on our analyses, Li is strongly coupled to Al within the quartz grains, which diffuses much more slowly compared to Li. Also, since the atomic ratio of Li/Al is less than one, other ions are likely occupying sites within the quartz for charge balance purposes, which could hinder any uncoupled Li from diffusing as quickly. Estimating ^{6}Li vs ^{7}Li diffusivity requires knowledge of β in Eq. (1), which is also unfortunately unconstrained. Thus, instead of assuming a value for β, we generated models over a range of β. We show that the isotopic excursions and concentration profiles can be modeled with a β of ~0.138 for an elapsed nondimensional time of ~0.0019 in Fig. 8. Time is nondimensionalized by $\tau = (180 \times 10^{-6})^2 / D_{7Li}$, where the numerator is the diffusion lengthscale in meters, and the denominator is the ^{7}Li diffusivity. Diffusivity values similar to Verhoogen (1952) result in fast diffusion times. If Li diffuses orders of magnitude slower due to coupling or competition with other ions, then the diffusion time will be longer. As diffusivity is strongly temperature dependent (e.g. Verhoogen, 1952), the exact value has implications for the closure temperature—when Li effectively no longer diffuses. Slower diffusivities allow for a slower cooling rate of the pegmatite. Yet, values closer to that predicted by Verhoogen (1952), indicate rapid cooling or a fundamental change in the diffusion mechanism.

In any case, if solid-state diffusion is responsible for the local isotopic excursion seen at the color zone transitions, the implication is that Li can diffuse even if Al, a much slower diffusing element (Tailby et al., 2018), does not. As discussed in a previous section, we suggested that Li substitution may be limited by the presence of Al in quartz. However, given that Al is often in excess, Li may still be free to diffuse, provided there are available sites. In this context, it is noteworthy that solid-state diffusion occurs across the white and orange zones in D but appears to be in the opposite direction in F, hinting at uphill diffusion occurring. Across the white to orange transition in F, heavier δ^{7}Li exists on the lower concentration side with a lower δ^{7}Li dip on the higher concentration side (the opposite of Fig. 8). Competition with monovalent cations (e.g. H^+) may dictate which way Li diffuses, and Li has been known to diffuse against its concentration gradient to provide

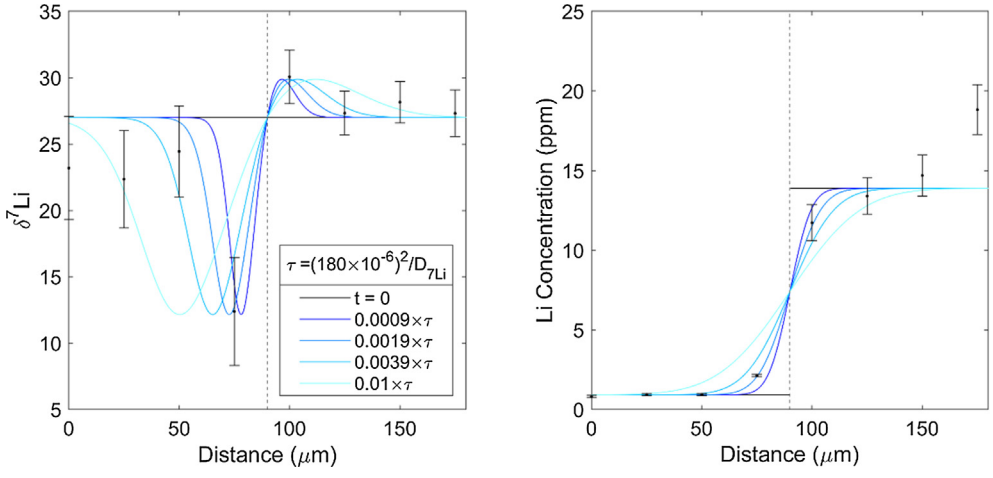

Fig. 8. Solid-state diffusion model for crystal D. Across the white to orange transition in crystal D is a rise in Li concentration and a downward excursion in isotope ratio on the low concentration side of the transition. This may be due to solid state diffusion of Li within the quartz, where ^{6}Li diffuses faster than ^{7}Li. Each line denotes a nondimensional diffusion time, as we do not know the exact Li diffusivities. Nondimensional time can be converted to seconds, assuming a diffusivity in m^2 s^{-1}, using $\tau = (180 \times 10^{-6})^2 / D_{7Li}$. We also assume a β value of 0.138. Error bars are $2 \times \sqrt{\sigma_{slope}{}^2 + \sigma_{counts}{}^2}$, where σ_{slope} is the standard error of the conversion factor from the number of counts/current to concentration, and σ_{counts} is the standard error of the number of counts/current. (For interpretation of the references to color in this figure legend, the reader is referred to the web version of this article.)

charge balance (e.g., Tollan et al., 2019). The Li/Al ratios in D are much lower than in F, which is consistent with the notion that there are available sites to diffuse in D but not in F. The paucity of lower Li/Al ratios in the white zone of F could indicate excess charge imbalance, which led to uphill diffusion. Nevertheless, Li concentration gradients remain, and they tend to mimic Al, leading us to believe Li diffusion effectively stopped after encountering Al. A similar phenomenon was observed with Li in zircons (Tang et al., 2017). Also, Li diffusion in olivine has been shown to follow slow and fast pathways (Dohmen et al., 2010). If such pathways exist in quartz, then the remaining Li concentration gradients may be indicators of the slow diffusion pathway.

6. Implications and conclusions

We found neither crystal growth fractionation nor Rayleigh distillation alone can completely capture the observed isotopic ratios or concentrations in the quartz. While rapid crystal growth (compared to diffusive transport of Li in the fluid) is needed to explain enrichments in Li concentration—through enrichments of Al (Phelps et al., 2020)—and can explain some of the variation in δ^7Li, unreasonably large differences in isotope diffusivity are required to reproduce the highest observed δ^7Li values on the rim for the same assumed growth rates. On the other hand, Rayleigh distillation can more easily explain how the isotopic ratios evolve, yet the observed jumps in concentration are not compatible with the steady progression predicted by fractional crystallization. In terms of δ^7Li vs Li concentration, we would expect complicated relationships if the isotopic profiles were dominantly growth rate driven. As Li concentration is governed by Al uptake, a disconnect between the isotopic profile and the concentration would give variable δ^7Li vs Li slopes. With Rayleigh distillation, we expect linear trends in δ^7Li vs Li, which is similar to our observations, although more complicated relationships are also observed (particularly for crystal F). We thus propose that a combination of both rapid growth and Rayleigh fractionation may be reflected in the elemental and isotopic zoning of the pegmatite quartzes. We suggest that Li isotopes are more sensitive to processes that change the composition of the whole system while trace element concentrations are more sensitive to local boundary layer effects at the grain scale.

Since our Rayleigh distillation modeling can only differentiate the fraction of Li remaining, we cannot necessarily tie this to the total pegmatite crystal fraction. Nevertheless, to achieve such large changes in Li isotopes from core to rim in the quartz, requires extensive crystallization *during* the growth of the quartz crystal. In a previous study, we showed that these quartz crystals formed within a day. If so, this would imply that miarolitic cavities hosting the quartz solidified quickly as well. Our results thus have implications for how quickly the last stages of a pegmatite crystallize. Measuring Li isotopes in other minerals in the miarolitic cavity would go far in testing this hypothesis. These measurements would also allow us to test whether the δ^7Li differences between crystals could be caused by heterogeneity within the chimney or if multiple crack opening events occurred.

Finally, the remarkably broad isotopic signatures seen here indicate that late stage magmatic or hydrothermal processes can lead to extreme Li isotopic fractionation from the scale of a mineral grain to the scale of a small magmatic body. These processes are all internal to the magmatic system, thus care must be taken when interpreting the Li isotopic composition of magmas as reflecting source composition or evidence of mixing.

Data availability

Data has been included as a supplementary file

Declaration of Competing Interest

The authors declare that they have no known competing financial interests or personal relationships that could have appeared to influence the work reported in this paper.

Acknowledgements

This work was supported by NSF-EAR 1753599 to C.-T.A.L We thank Dr. Yunbin Guan from Caltech for his assistance in making measurements. Discussions with Blue Sheppard were appreciated. This paper is dedicated to the late Douglas M. Morton for inspiring our interests in pegmatites.

Appendix A. Supplementary material

Supplementary material to this article can be found online at https://doi.org/10.1016/j.gca.2022.09.014.

References

Bearman, R.J., Jolly, D.L., 1981. Mass dependence of the self diffusion coefficients in two equimolar binary liquid Lennard-Jones systems determined through molecular dynamics simulation. Mol. Phys. 44, 665–675.
Bell, D.R., Hervig, R.L., Buseck, P.R., Aulbach, S., 2009. Lithium isotope analysis of olivine by SIMS: Calibration of a matrix effect and application to magmatic phenocrysts. Chem. Geol. 258, 5–16.
Cashman, K.V., 1993. Relationship between plagioclase crystallization and cooling rate in basaltic melts. Contrib. Mineral. Petrol. 113, 126–142.
Chadwick, R.A., 1958. Mechanisms of pegmatite emplacement. Geol. Soc. Am. Bull. 69, 803–836.
Chakoumakos, B.C., Lumpkin, G.R., 1990. Pressure-Temperature Constraints on the Crystallization of the Harding Pegmatite, Taos County, New Mexico. Can. Mineral. 28, 287–298.
Deubener, J., Sternitzke, M., Mueller, G., 1991. Feldspars MAlSi3O8 (M= H, Li, Ag) synthesized by low-temperature ion exchange. Am. Mineral. 76, 1620–1627.
Dohmen, R., Kasemann, S.A., Coogan, L., Chakraborty, S., 2010. Diffusion of Li in olivine. Part I: Experimental observations and a multi species diffusion model. Geochim. Cosmochim. Acta 74, 274–292.
Eiler, J.M., Graham, C., Valley, J.W., 1997. SIMS analysis of oxygen isotopes: matrix effects in complex minerals and glasses. Chem. Geol. 138, 221–244.
Fritz, S.J., 1992. Measuring the ratio of aqueous diffusion coefficients between 6Li +Cl− and 7Li+Cr− by osmometry. Geochim. Cosmochim. Acta 56, 3781–3789.
Götze, J., Plötze, M., Habermann, D., 2001. Origin, spectral characteristics and practical applications of the cathodoluminescence (CL) of quartz - a review. Mineral. Petrol. 71, 225–250.
Götze, J., Plötze, M., Trautmann, T., Götze, J., Plötze, M., Trautmann, T., 2005. Structure and luminescence characteristics of quartz from pegmatites. Am. Mineral. 90, 13–21.
Hoover, W.F., Penniston-Dorland, S.C., Baumgartner, L.P., Bouvier, A., Baker, D., Dragovic, B., Gion, A., 2021. A Method for Secondary Ion Mass Spectrometry Measurement of Lithium Isotopes in Garnet: The Utility of Glass Reference Materials. Geostand. Geoanalytical Res. 45, 477–499.
Jaeger, J.C., Carslaw, H.S., 1959. Conduction of Heat in Solids. Clarendon P.
Jahns, R.H., Burnham, C.W., 1969. Experimental studies of pegmatite genesis; l, A model for the derivation and crystallization of granitic pegmatites. Econ. Geol. 64, 843–864.
Jahns, R.H., Wright, L.A., 1951. Gem-and lithium-bearing pegmatites of the Pala district, San Diego County, California. State of California, Department of Natural Resources, Division of Mines.
Jambon, A., 1980. Isotopic fractionation: A kinetic model for crystals growing from magmatic melts. Geochim. Cosmochim. Acta 44, 1373–1380.
Jochum, K.P., Willbold, M., Raczek, I., Stoll, B., Herwig, K., 2005. Chemical Characterisation of the USGS Reference Glasses GSA-1G, GSC-1G, GSD-1G, GSE-1G, BCR-2G, BHVO-2G and BIR-1G Using EPMA, ID-TIMS, ID-ICP-MS and LA-ICP-MS. Geostand. Geoanalyt. Res. 29, 285–302.
Kunze, R.W., Fuoss, R.M., 1962. Conductance of the alkali halides. III. The isotopic lithium chlorides 1. J. Phys. Chem. 66, 930–931.
London, D., Kontak, D.J., 2012. Granitic pegmatites: scientific wonders and economic bonanzas. Elements 8, 257–261.
Lynton, S.J., Walker, R.J., Candela, P.A., 2005. Lithium isotopes in the system Qz-Ms-fluid: An experimental study. Geochim. Cosmochim. Acta 69, 3337–3347.
Lyubartsev, A.P., Laasonen, K., Laaksonen, A., 2001. Hydration of Li+ ion. An ab initio molecular dynamics simulation. J. Chem. Phys. 114, 3120–3126.
Maloney, J.S., Nabelek, P.I., Sirbescu, M.-L.-C.-H., 2008. Lithium and its isotopes in tourmaline as indicators of the crystallization process in the San Diego County pegmatites, California, USA. *Eur. J. Mineral.* 20, 905–916.

Marschall, H.R., Pogge von Strandmann, P.A.E., Seitz, H.-M., Elliott, T., Niu, Y., 2007. The lithium isotopic composition of orogenic eclogites and deep subducted slabs. Earth Planet. Sci. Lett. 262, 563–580.
Morton, D.M., Sheppard, J.B., Miller, F.K., Lee, C.A., 2018. Petrogenesis of the cogenetic Stewart pegmatite-aplite, Pala, California: Regional implications. Lithosphere 11, 91–128.
Nash, W.P.P., Crecraft, H.R.R., 1985. Partition coefficients for trace elements in silicic magmas. Geochim. Cosmochim. Acta 49, 2309–2322.
Neukampf, J., Ellis, B.S., Magna, T., Laurent, O., Bachmann, O., 2019. Partitioning and isotopic fractionation of lithium in mineral phases of hot, dry rhyolites: The case of the Mesa Falls Tuff, Yellowstone. *Chem. Geol.* 506, 175–186.
Nigrini, A., 1970. Diffusion in rock alteration systems; I, Prediction of limiting equivalent ionic conductances at elevated temperatures. Am. J. Sci. 269, 65–91.
Pearce, N.J.G.G., Perkins, W.T., Westgate, J.A., Gorton, M.P., Jackson, S.E., Neal, C.R., Chenery, S.P., 1997. A Compilation of New and Published Major and Trace Element Data for NIST SRM 610 and NIST SRM 612 Glass Reference Materials. Geostand. Geoanalyt. Res. 21, 115–144.
Penniston-Dorland, S., Liu, X.-M.-M., Rudnick, R.L., 2017. Lithium isotope geochemistry. Rev. Miner. Geochem. 82, 165–217.
Phelps, P.R., Lee, C.-T.-T.-A., Morton, D.M., 2020. Episodes of fast crystal growth in pegmatites. Nat. Commun. 11, 1–10.
Qi, H.P., Taylor, P.D.P., Berglund, M., De Bièvre, P., 1997. Calibrated measurements of the isotopic composition and atomic weight of the natural Li isotopic reference material IRMM-016. Int. J. Mass Spectrom. Ion Process. 171, 263–268.
Richter, F.M., Davis, A.M., DePaolo, D.J., Watson, E.B., 2003. Isotope fractionation by chemical diffusion between molten basalt and rhyolite. Geochim. Cosmochim. Acta 67, 3905–3923.
Richter, F.M., Mendybaev, R.A., Christensen, J.N., Hutcheon, I.D., Williams, R.W., Sturchio, N.C., Beloso, A.D., Beloso Jr, A.D., Beloso, A.D., Beloso Jr, A.D., 2006. Kinetic isotopic fractionation during diffusion of ionic species in water. Geochim. Cosmochim. Acta 70, 277–289.
Sartbaeva, A., Wells, S.A., Redfern, S.A.T., 2004. Li + ion motion in quartz and β-eucryptite studied by dielectric spectroscopy and atomistic simulations. J. Phys. Condens. Matter 16, 8173–8189.
Simmons, W.B., Webber, K.L., 2008. Pegmatite genesis: state of the art. Eur. J. Mineral. 20, 421–438.
Smith, V.G., Tiller, W.A.A., Rutter, J.W., 1955. A mathematical analysis of solute redistribution during solidification. Can. J. Phys. 33, 723–745.
Tailby, N.D., Cherniak, D.J., Watson, E.B., 2018. Al diffusion in quartz. Am. Mineral. 103, 839–847.
Tang, M., Rudnick, R.L., McDonough, W.F., Bose, M., Goreva, Y., 2017. Multi-mode Li diffusion in natural zircons: Evidence for diffusion in the presence of step-function concentration boundaries. Earth Planet. Sci. Lett. 474, 110–119.
Tang, Y.-J., Zhang, H.-F., Ying, J.-F., 2007. Review of the Lithium Isotope System as a Geochemical Tracer. Int. Geol. Rev. 49, 374–388.
Teng, F.-Z., McDonough, W.F., Rudnick, R.L., Walker, R.J., 2006a. Diffusion-driven extreme lithium isotopic fractionation in country rocks of the Tin Mountain pegmatite. Earth Planet. Sci. Lett. 243, 701–710.
Teng, F.-Z., McDonough, W.F., Rudnick, R.L., Walker, R.J., Sirbescu, M.-L.-C., 2006b. Lithium isotopic systematics of granites and pegmatites from the Black Hills, South Dakota. Am. Mineral. 91, 1488–1498.
Tiller, W.A., Jackson, K.A., Rutter, J.W., Chalmers, B., 1953. The redistribution of solute atoms during the solidification of metals. Acta Metall. 1, 428–437.
Tollan, P., Ellis, B., Troch, J., Neukampf, J., 2019. Assessing magmatic volatile equilibria through FTIR spectroscopy of unexposed melt inclusions and their host quartz: a new technique and application to the Mesa Falls Tuff, Yellowstone. Contrib. Mineral. Petrol. 174, 24.
Tomascak, P.B., Magna, T., Dohmen, R., 2016. Advances in Lithium Isotope Geochemistry. Springer International Publishing, Cham.
Verhoogen, J., 1952. Ionic diffusion and electrical conductivity in quartz. Am. Mineral. J. Earth Planet. Mater. 37, 637–655.
Wark, D.A., Watson, E.B., 2006. TitaniQ: A titanium-in-quartz geothermometer. Contrib. Mineral. Petrol. 152, 743–754.
Watkins, J.M., DePaolo, D.J., Watson, E.B., 2017. Kinetic fractionation of non-traditional stable isotopes by diffusion and crystal growth reactions. Rev. Mineral. Geochem. 82, 85–125.
Watson, E.B., Müller, T., 2009. Non-equilibrium isotopic and elemental fractionation during diffusion-controlled crystal growth under static and dynamic conditions. Chem. Geol. 267, 111–124.
Webber, K.L., Simmons, W.B., Falster, A.U., Foord, E.E., 1999. Cooling rates and crystallization dynamics of shallow level pegmatite-aplite dikes, San Diego County, California. *Am. Mineral.* 84, 708–717.
Winkler, H.G.F., 1949. Crystallization of basaltic magma as recorded by variation of crystal-size in dikes. Mineral. Mag. J. Mineral. Soc. 28, 557–574.
Wunder, B., Meixner, A., Romer, R.L., Heinrich, W., 2006. Temperature-dependent isotopic fractionation of lithium between clinopyroxene and high-pressure hydrous fluids. Contrib. Mineral. Petrol. 151, 112–120.
Wunder, B., Meixner, A., Romer, R.L., Feenstra, A., Schettler, G., Heinrich, W., 2007. Lithium isotope fractionation between Li-bearing staurolite, Li-mica and aqueous fluids: An experimental study. Chem. Geol. 238, 277–290.
Zhang, Y., 2008. Geochemical Kinetics. Princeton University Press.